ORIGINAL PAPER

Research on performance of thermal management system integrated with multiple heat exchange methods

Luo Zhang[1] · **Qiuqi Yuan**[2] · **Song Hu**[1] · **Xiaoming Xu**[1]

Abstract

A good thermal management system can effectively improve the performance of the lithium-ion battery and ensure the thermal safety of the lithium-ion battery. Therefore, based on the heat-generating characteristics of lithium-ion batteries obtained above, this paper established a composite thermal management system including heat pipes, thermally conductive silica gel, phase change materials, and microchannel liquid cooling plates. The velocity uniformity coefficient, friction resistance coefficient, and thermal characteristic parameters are used as evaluation indicators, and the thermal management system inlet flow is optimized to obtain the optimal inlet flow of the thermal management system. Based on this, the thermal management capability of the established thermal management system under different operating conditions of the lithium-ion battery is analyzed. It is advisable to select 0.67L/min as the inlet flow rate of the microchannel liquid-cooled plate of the composite thermal management system.

Keywords Li-ion battery · Thermal management system · PCM · Heat pipe · Microchannel

Introduction

New energy vehicles mainly include electric vehicles, fuel cell vehicles, etc. Due to the high cost of fuel cells, electric vehicles are currently the main carrier of new energy vehicles [1–3]. As the key component of electric vehicles, power batteries are the source of power for the entire electric vehicle. The ternary lithium-ion battery composed of Ni/Co/Mn three elements has a high-energy density, which can effectively increase the cruising range of electric vehicles [4].

At present, power battery thermal management systems (TMS) mainly include air cooling, liquid cooling, heat pipe cooling, and phase change material cooling [5]. Among them, the air-cooled heat management system has a simple configuration and low cost [6]. It has been used in early electric vehicle power battery systems, but

✉ Song Hu
  husong_90@163.com

✉ Xiaoming Xu
  xuxiaoming3777ustb@163.com

1 University of Science and Technology Beijing, Beijing, China

2 Jiangsu University, Zhenjiang, China

its heat dissipation efficiency is low, and it cannot meet the heat dissipation requirements of current power batteries during high-rate charging and discharging. There are few studies on the air-cooling and heat management system for power batteries [7–10]. Huo et al. [11] established a direct current (DC) liquid cooling system, using a combination of experiment and simulation to study the cooling of the liquid cooling system when the power battery is discharged at 5C. The results show that the flow of coolant will affect the heat transfer capacity of the liquid cooling plate; Jarrett et al. [12] designed a U-shaped liquid cooling plate and analyzed the influence of the width and position of the flow channel on the internal heat transfer process of the liquid cooling system. They found that the U-shaped liquid-cooled plate can improve the uniformity of the temperature distribution of the power battery module. Putra et al. [13] studied the influence of distilled water, alcohol, acetone, and other working fluids on the heat dissipation capacity of flat heat pipes. The heat management system of the heat pipe has the best heat dissipation capacity; Tran et al. [14] used an experimental method to study the influence of the position angle of the heat pipe in the thermal management system on the heat transfer process. The research results show that the position angle is different on the overall thermal management system.

The effect of cooling capacity is small, but it has a greater effect on the temperature difference inside the power battery module. Javani et al. [15] analyzed the influence of the thickness of the phase change material on the internal thermal management system. With the influence of the heat transfer process, they found that when the thickness of the phase change material is 3mm, the heat transfer rate is fastest; Wilke et al. [16] applied paraffin/expanded graphite composite phase change material to the lithium-ion battery puncture experiment, and they found that the paraffin/expanded graphite composite phase change material can inhibit the temperature diffusion at the perforation of the lithium-ion battery. Kong et al. [17] proposed a thermal management system that combines liquid cooling and phase change materials and studied its heat dissipation capacity. They found that the thermal management system can keep the temperature of the lithium iron phosphate battery at 3C discharge. Below 312K, Bai et al. [18] established a two-dimensional lithium-ion battery model to analyze the heat dissipation capacity of a thermal management system coupled with heat pipes and phase change materials. They found that compared to a single cooling method, a composite thermal management system can improve power and the uniformity of the temperature distribution of the battery module.

In summary, domestic and foreign researchers have designed different composite thermal management systems, such as phase change material/liquid cooling composite thermal management systems and phase change material/heat pipe composite thermal management systems. Existing studies have shown that, compared to a single thermal management method, the use of a composite thermal management system can achieve different cooling methods to "complement each other's strengths" and meet the heat dissipation requirements of the power battery system under complex working conditions. Therefore, it is still the focus and difficulty of current research to establish an appropriate composite thermal management system to meet the heat dissipation requirements of the power battery system under complex working conditions [19–22].

This paper attempts to make several original contributions and improvements to the current research as shown in the following:

1) Presented a thermal management system, which can simultaneously meet the requirements of high-speed discharge, abuse, and heating of power battery system under low-temperature environment.
2) The changes of the overall average temperature and the temperature difference between the maximum and minimum temperature of the Li-ion battery module under different liquid inlet flow rates of the thermal management system were studied.

3) The flow rate of 0.67L/min was selected as the best liquid inlet flow rate by velocity uniformity coefficient, friction coefficient, and thermal characteristics.

Model structure

Geometry

In this research, a three-dimensional model of a composite thermal management system was established, as shown in Fig. 1. The model mainly includes six lithium-ion batteries (numbered Cell#1–#6), heat pipes, thermal silica gel, side microchannel liquid cooling plates, phase change materials, and bottom microchannel liquid cooling plates. The lithium-ion battery model is established based on the 50Ah LiNi0.8Co0.1Mn0.1O2 (NCM) lithium-ion battery used in the experiment, and the geometric dimensions are the same. There are three heat pipes and two parts of thermally conductive silica gel between the lithium-ion battery. The evaporation section of the heat pipe is attached to the surface of the battery, and the thermally conductive silica gel is distributed between the battery and the heat pipe. The condensing section of the heat pipe is embedded in the phase change material. The phase change material is attached to the microchannel liquid cooling plate at the bottom. There are 18 pipelines inside the microchannel liquid cooling plate, one end is a volume flow inlet, and the other end is a pressure outlet. The side microchannel liquid-cooling plates are "S"-shaped, which are symmetrically distributed at both ends of the lithium-ion battery. In order to improve the uniformity of the temperature distribution of the lithium-ion battery, the volumetric flow inlet directions of the two-side microchannel liquid-cooling plates are opposite.
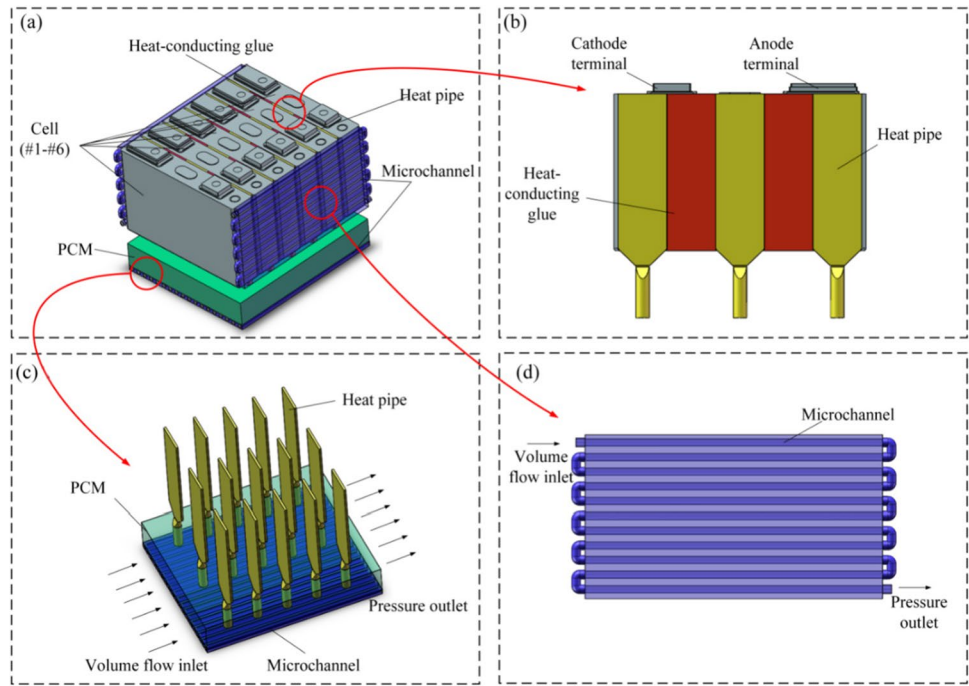
The geometric dimensions of thermal manage system, lithium-ion batteries, side microchannel, and heat pipe are shown in Table 1. In addition, the liquid in the microchannel liquid-cooled plate is 50% ethylene glycol solution. The specific heat of glycol solution is 3.281 (kJ/kg·K), and its thermal conductivity is 0.38 (W/m·K). And the heat pipe in the model is sintered without coolant inside.

Mathematical model

The heat transfer process of the thermal management system can be regarded as a three-dimensional unsteady heat conduction process. The heat transfer process of the established three-dimensional model of the thermal management system can be expressed by Eq. (1) [23]:

$$\rho_v C \frac{\partial T}{\partial \tau} = q_v + \frac{\partial}{\partial x}\left(k_x \frac{\partial T}{\partial x}\right) + \frac{\partial}{\partial y}\left(k_y \frac{\partial T}{\partial y}\right) + \frac{\partial}{\partial z}\left(k_z \frac{\partial T}{\partial z}\right)$$

(1)

Fig. 1 Geometric model of the thermal management system. **a** Thermal management system assembly; **b** heat-conducting structure between the cells; **c** the coupling structure of PCM and microchannel; **d** side microchannel

Table 1 Geometric dimensions of components

Features	Length (mm)	Width (mm)	Height (mm)	Diameter (mm)
Thermal manage system	150	130	125	-
Lithium-ion batteries	143	20	90	-
Side microchannel	-	-	-	4
Heat pipe	28	2	120	2

In the formula, ρ_v represents the density of the component, C represents the specific heat capacity of the component, $\partial T/\partial \tau$ represents the rate of temperature rise, q_v represents the volume heat production rate, and k_x, k_y, and k_z are the thermal management systems in x, y, Thermal conductivity in the z-direction.

The fluid in the liquid-cooled plate is a mixed solution of ethylene glycol, which belongs to Mach number fluid flow, and can be treated as an incompressible fluid. The density of the fluid does not change with time. The mass conservation equation can be expressed by Eq. (2) [24]:

$$\frac{\partial \rho}{\partial t} + \frac{\partial(\rho u)}{\partial x} + \frac{\partial(\rho v)}{\partial y} + \frac{\partial(\rho w)}{\partial z} = 0 \tag{2}$$

where ρ is the fluid density and u, v, and w are the velocity vector components on the coordinate axis, respectively.

In this study, the ethylene glycol mixed solution is an incompressible fluid with constant viscosity, and the momentum conservation equation can be simplified to Formula (3) [25]:

x-direction:

$$\frac{\partial U}{\partial t} + u\frac{\partial U}{\partial x} + v\frac{\partial U}{\partial y} + w\frac{\partial U}{\partial z} = F_x - \frac{1}{\rho}\frac{\partial p}{\partial x} + \frac{\mu}{\rho}\left(\frac{\partial^2 u}{\partial x^2} + \frac{\partial^2 u}{\partial y^2} + \frac{\partial^2 u}{\partial z^2}\right) \tag{3a}$$

y-direction:

$$\frac{\partial v}{\partial t} + u\frac{\partial v}{\partial x} + v\frac{\partial v}{\partial y} + w\frac{\partial v}{\partial z} = F_y - \frac{1}{\rho}\frac{\partial p}{\partial y} + \frac{\mu}{\rho}\left(\frac{\partial^2 v}{\partial x^2} + \frac{\partial^2 v}{\partial y^2} + \frac{\partial^2 v}{\partial z^2}\right) \tag{3b}$$

z-direction:

$$\frac{\partial w}{\partial t} + u\frac{\partial v}{\partial x} + v\frac{\partial v}{\partial y} + w\frac{\partial v}{\partial z} = F_z - \frac{1}{\rho}\frac{\partial p}{\partial z} + \frac{\mu}{\rho}\left(\frac{\partial^2 w}{\partial x^2} + \frac{\partial^2 w}{\partial y^2} + \frac{\partial^2 w}{\partial z^2}\right) \tag{3c}$$

In the formula, F_x, F_y, and F_z are the components of the volume force in the x, y, and z directions; p is the pressure acting on the micro-element body; and u, v, and w

are the velocity vector components on the coordinate axis, respectively.

The established thermal management system follows the first law of thermodynamics, and the energy conservation equation is shown in Eq. (4) [26]:

$$\frac{\partial(\rho T)}{\partial t} + \frac{\partial(\rho u T)}{\partial x} + \frac{\partial(\rho v T)}{\partial y} + \frac{\partial(\rho w T)}{\partial z} =$$
$$\frac{\partial}{\partial x}\left(\frac{k_{Lq}}{C_{Lq}}\frac{\partial T}{\partial x}\right) + \frac{\partial}{\partial x}\left(\frac{k_{Lq}}{C_{Lq}}\frac{\partial T}{\partial x}\right) + \frac{\partial}{\partial x}\left(\frac{k_{Lq}}{C_{Lq}}\frac{\partial T}{\partial x}\right) + S_T \quad (4)$$

In the formula, k_{Lq} is the thermal conductivity of the fluid, T is the temperature, C_{Lq} is the specific heat capacity of the fluid, and S_T is the heat source in the fluid.

For the glycol mixed solution flowing in the liquid cooling plate, due to the relatively high flow rate and the complicated internal structure of the liquid cooling plate, the flow state is changeable, the fluctuation is large, and turbulence is easily formed. In this study, turbulent kinetic energy model (k model) is used to deal with this.

Among them, the k equation, the turbulent kinetic energy equation, is shown in Equation (5) [27]:

$$\rho\frac{\partial k}{\partial t} + \rho u_j\frac{\partial k}{\partial x_j} = \frac{\partial}{\partial x_j}\left[\left(\mu + \frac{\mu_t}{\sigma_k}\right)\frac{\partial k}{\partial x_j}\right] + \mu_t\frac{\partial u_i}{\partial x_j}\left(\frac{\partial u_i}{\partial x_j} + \frac{\partial u_j}{\partial x_i}\right) - \rho\varepsilon \quad (5)$$

ε is the turbulent dissipation rate, as shown in Equation (6):

$$\rho\frac{\partial\varepsilon}{\partial t} + \rho u_k\frac{\partial\varepsilon}{\partial x_k} = \frac{\partial}{\partial x_k}\left[\left(\mu + \frac{\mu_t}{\sigma_\varepsilon}\right)\frac{\partial\varepsilon}{\partial x_k}\right] + \frac{c_1}{k}\mu_t\frac{\partial u_i}{\partial x_j}\left(\frac{\partial u_i}{\partial x_j} + \frac{\partial u_j}{\partial x_i}\right) - c_2\rho\frac{\varepsilon^2}{k} \quad (6)$$

Among them, the turbulent viscosity coefficient μ_t is shown in Formula (7) [28]:

$$\mu_t = \frac{c_\mu\rho k^2}{\varepsilon} \quad (7)$$

In the formula, u_k and ρ is the P_r numbers of k and ε, respectively; μ_t is the turbulent viscosity; and c_μ, $c1$, and $c2$ are empirical constants.

Boundary conditions

The simulations in this study were carried out with an initial temperature condition of 20°C and a lithium battery discharge multiplier of 1 C. Since the heat generation rate varies depending on the operating condition of the battery, the heat generation rate model from the literature by Bernardi D et al [29] was chosen for the heat generation rate estimation as shown in Equation (8). The inlet water flow rates for the cooling system used were 0.33 L/min, 0.50 L/min, 0.67/min, and 0.83 L/min.

The internal heat transfer form of the established thermal management system model is heat conduction, and the

heat exchange form with the external environment is thermal radiation, as shown in Fig. 2. Analyze the heat transfer process of the established thermal management system in two environments. First, at normal ambient temperature, the lithium-ion battery is discharged at different discharge rates with or without an external heat source. At this time, the heat is The electric core generates, the part where the heat pipe connects with the surface of the electric core is an evaporation section that absorbs heat, and the part where the heat pipe connects with the phase change material is a condensation section that releases heat. In a low-temperature environment, the lithium-ion battery does not work. At this time, the heat is provided by the ethylene glycol mixed solution. The part connecting the heat pipe and the phase change material is the evaporation section that absorbs heat, and the part connecting the heat pipe and the battery is a condensation section that releases heat.

$$q = \frac{I}{V_b}\left(U - U_0 + T\frac{dU_0}{dT}\right) \quad (8)$$

where V_b is the volume of the lithium battery unit, I is the charge/discharge current, U is the battery unit voltage (3.5V in this model), U_0 is the open circuit voltage, T is the temperature, $\frac{dU_0}{dT}$ is the temperature coefficient, and $(U - U_0)/V_b, T\frac{dU_0}{dT}/V_b$ are the Joule heat and reversible reaction heat, respectively.

Results and discussion

Performance analysis of thermal management system under different inlet liquid flow
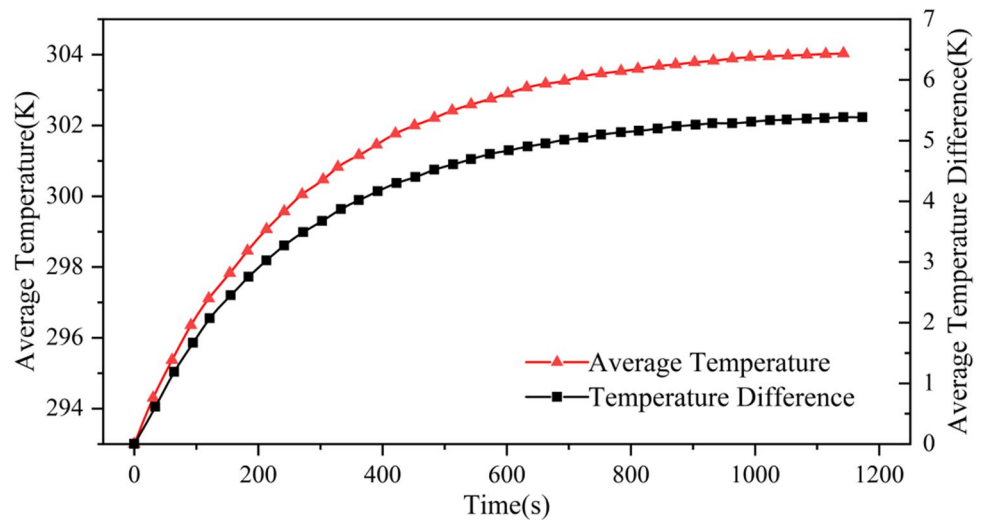
(1) Analysis of thermal parameters of thermal management system at 0.33L/min inlet flow

Figure 3 shows the overall average temperature of the Li-ion battery module and the temperature difference between the maximum and minimum temperature of the Li-ion battery module at an inlet flow rate of 0.33L/min. As shown in the graph, the lithium-ion battery module discharges to a faster average temperature rise rate in the first 500s and slows down and stabilizes after 1000s. At the end of discharge, the average temperature of the battery module is 303.9K. This is because the heat management system has a low liquid inlet speed, and the actual heat exchange area between the liquid cooling plate and the battery module increases slowly. In the early stage of lithium-ion battery discharge, the heating battery cannot be dissipated in time, which causes the overall temperature of the battery module to rise. Faster, and then as the ethylene glycol mixed solu-
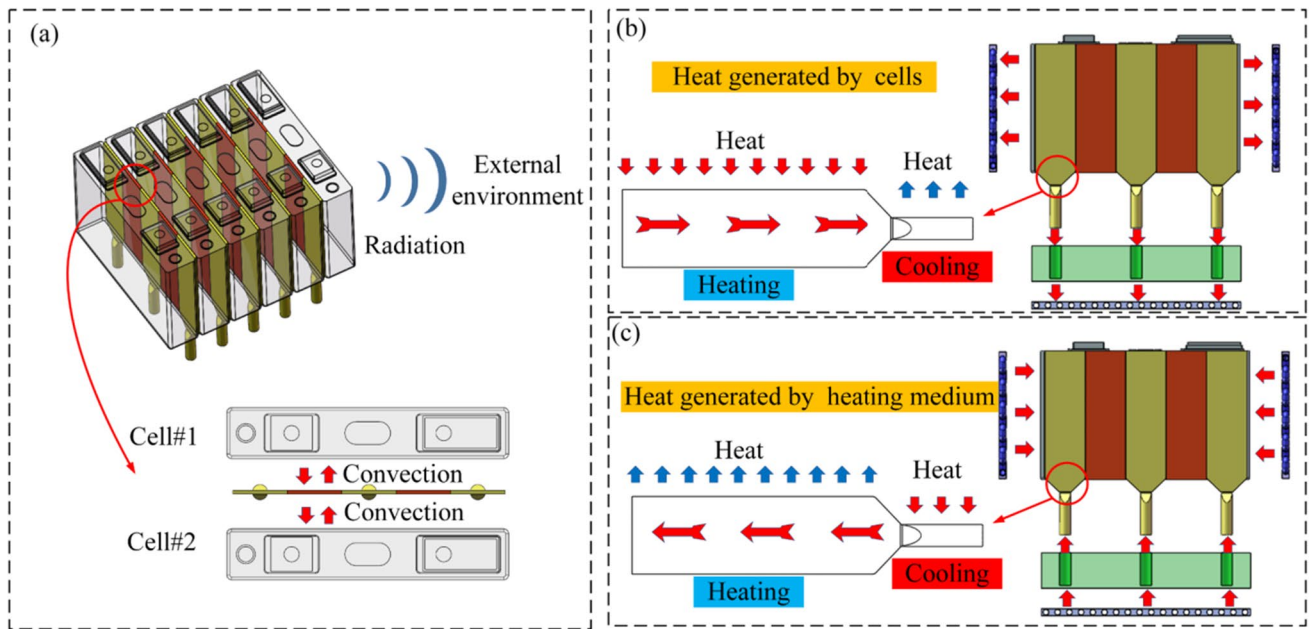
Fig. 2 Thermal management system boundary conditions. **a** Cell boundary conditions; **b** normal ambient temperature condition, and **c** low ambient temperature condition.

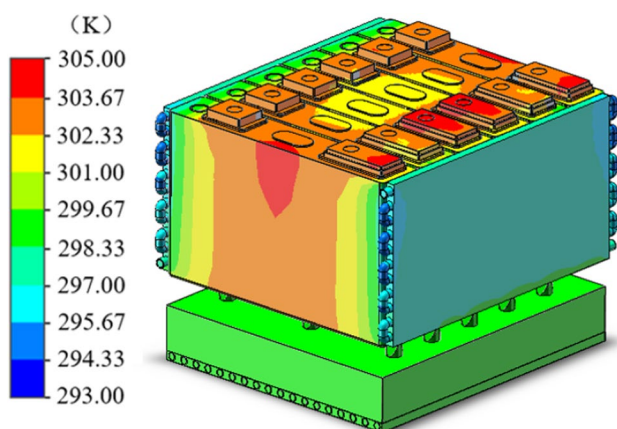**Fig. 3** Average temperature and temperature difference of battery modules at the inlet flow rate of 0.33L/min

tion fills the microchannel liquid cooling plate, the heat exchange area between the heat dissipation medium and the battery increases to the maximum, and the overall temperature of the lithium-ion battery module tends to stabilize. Similarly, for the average temperature difference of the lithium-ion battery during the discharge process, due to the partial heat exchange between the thermal management system and the battery module in the early stage, the internal temperature difference of the battery module rises quickly. After the discharge is carried out for 800s, the average temperature difference of the battery module tends to be stable. At the end

of discharge, the average temperature difference of the battery module is 5.2K.

Figure 3 shows the overall average temperature and temperature difference of the lithium-ion battery module under the 0.33L/min inlet flow rate. As shown in the figure, the average temperature rise rate of the lithium-ion battery module is faster before it is discharged to 500s, and it rises after 500s. The rate has slowed down and stabilized after 1000s. At the end of discharge, the average temperature of the battery module is 303.9K. This is because the heat management system has a low liquid inlet speed, and the actual heat exchange area

between the liquid cooling plate and the battery module increases slowly. In the early stage of lithium-ion battery discharge, the heating battery cannot be dissipated in time, which causes the overall temperature of the battery module to rise. Faster, and then as the ethylene glycol mixed solution fills the microchannel liquid cooling plate, the heat exchange area between the heat dissipation medium and the battery increases to the maximum, and the overall temperature of the lithium-ion battery module tends to stabilize. Similarly, for the average temperature difference of the lithium-ion battery during the discharge process, due to the partial heat exchange between the thermal management system and the battery module in the early stage, the internal temperature difference of the battery module rises quickly. After the discharge is carried out for 800s, the battery module the average temperature difference tends to be stable. At the end of discharge, the average temperature difference of the battery module is 5.2K.

Figure 4 is a cloud diagram of the overall temperature distribution of the thermal management system at the inlet flow rate of 0.33L/min. As shown in the figure, the high-temperature area of the thermal management system including the battery modules is concentrated in the middle and the positive and negative positions of the lithium-ion battery. This is related to the self-heating characteristics of lithium-ion batteries. As mentioned in the summary of 2.3.2, when the side reactions of lithium-ion batteries are not triggered, the high-temperature regions of lithium-ion batteries are concentrated at the positive and negative electrodes. This is due to the electrochemistry at the positive and negative electrodes caused by higher heat production. And because the two ends of the lithium-ion battery

**Fig. 4** Temperature distribution of TMS at the inlet liquid flow rate of 0.33L/min

are close to the side microchannel liquid-cooling plate in the thermal management system, the temperature in the middle position of the lithium-ion battery is higher than other positions under the influence of this. In addition, the position with the lowest temperature in the entire thermal management system is the "U"-shaped inflection point in the side microchannel liquid cooling plate. There is no direct contact with the battery, so the temperature is the lowest here.

Figure 4 is a cloud diagram of the overall temperature distribution of the thermal management system at the inlet flow rate of 0.33L/min. As shown in the figure, the high-temperature area of the thermal management system including the battery modules is concentrated in the middle and the positive and negative positions of the lithium-ion battery. This is related to the self-heating characteristics of lithium-ion batteries. As mentioned in the summary of 2.3.2, when the side reactions of lithium-ion batteries are not triggered, the high-temperature regions of lithium-ion batteries are concentrated at the positive and negative electrodes. This is due to the electrochemistry at the positive and negative electrodes caused by higher heat production. And because the two ends of the lithium-ion battery are close to the side microchannel liquid-cooling plate in the thermal management system, the temperature in the middle position of the lithium-ion battery is higher than other positions under the influence of this. In addition, the position with the lowest temperature in the entire thermal management system is the "U"-shaped inflection point in the side microchannel liquid cooling plate. There is no direct contact with the battery, so the temperature is the lowest here.

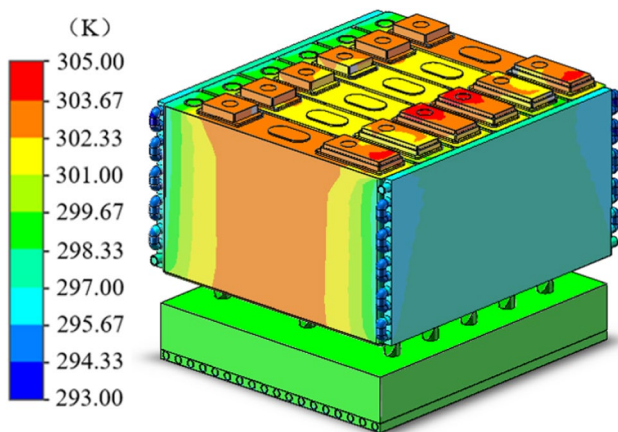(2) Analysis of thermal parameters of thermal management system at the inlet flow rate of 0.50L/min

Figure 5 shows the overall average temperature and the temperature difference between the maximum and minimum temperature of the Li-ion battery module under a 0.50L/min inlet flow rate. As shown in the figure, the average temperature rise rate of the lithium-ion battery module is faster before it is discharged to 600s, and it rises after 600s. The rate has slowed down and stabilized after 800s. When the discharge is cut off, the average temperature of the battery module is 302.1K. Similarly, the average temperature difference of lithium-ion battery modules also tends to rise rapidly and then stabilize. Compared with the temperature characteristics of the lithium-ion battery module at the inlet flow rate of 0.33L/min, it can be found that with the increase of the inlet flow rate, the changes of the average temperature and the average temperature difference of the lithium-ion battery module are narrowing, and the two values tend to be stable. This is due to the increase in the inlet flow rate and the increase in the speed at which the ethylene glycol mixed solution fills the microchannel liquid cooling plate. The heat exchange area of
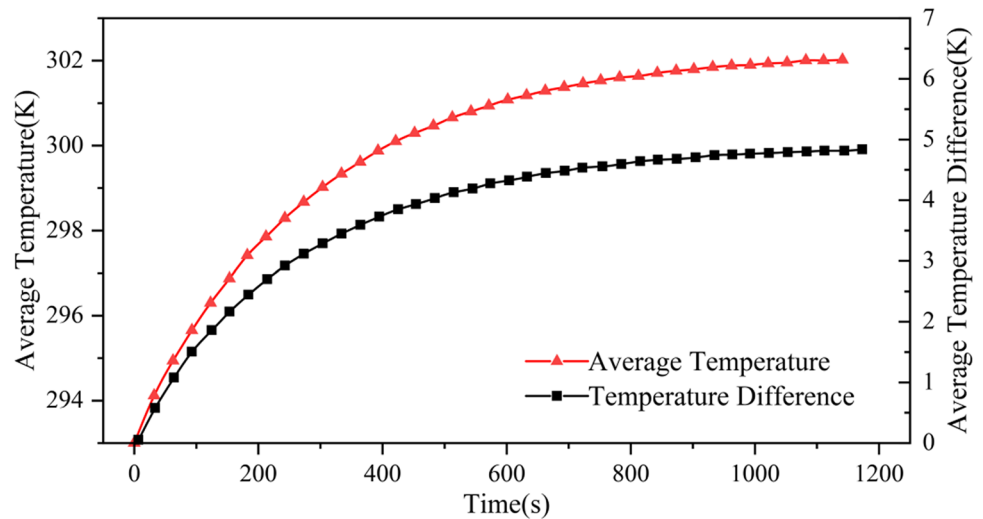
the microchannel liquid cooling plate and the lithium-ion battery module increases faster, resulting in an increase in heat exchange efficiency. The temperature difference within the battery is also reduced.

Figure 6 is a cloud diagram of the overall temperature distribution of the thermal management system at an inlet flow of 0.50L/min. As shown in the figure, due to the self-healing characteristics of the lithium-ion battery, the high-temperature area of the entire thermal management system is concentrated at the positive and negative electrodes of the lithium-ion battery. And with the increase of the inlet flow rate, the temperature distribution of the microchannel liquid-cooling plates located on both sides of the thermal management system tends to be more uniform, which results in the temperature distribution of the main body of the lithium-ion battery module that also tends to be uniform.

Fig. 6 Temperature distribution of TMS at the inlet liquid flow rate of 0.50L/min

(3) Analysis of thermal parameters of thermal management system at the inlet flow rate of 0.67L/min

Figure 7 shows the overall average temperature and the temperature difference between the maximum and minimum temperature of the Li-ion battery module under the 0.67L/min inlet flow rate. As shown in the figure, the average temperature of the lithium-ion battery module shows a rapid upward trend before being discharged to 500s, and after 500s, it tends to be stable. When the discharge ends, the average temperature of the battery module is 301.8K. Similarly, the average temperature difference of lithium-ion battery modules also tends to rise rapidly and then stabilized. Compared with the temperature change of the lithium-ion battery module at the inlet flow of 0.33L/min and 0.50L/min, the efficiency of the heat exchange area between the microchannel liquid cooling plate and the lithium-ion battery module is improved. At the same time, the changes of the average temperature and the average temperature difference tend to be more stable. Therefore, the lithium-ion battery module at the inlet flow rate of 0.67L/min is further advanced.

Figure 8 is a cloud diagram of the overall temperature distribution of the thermal management system at the inlet flow rate of 0.67L/min. As shown in the figure, compared with the temperature distribution of the thermal management system at the inlet flow rate of 0.33L/min and 0.50L/min, the high-temperature area of the lithium-ion battery module is further reduced, and the overall temperature distribution tends to be more uniform.

(4) Analysis of thermal parameters of thermal management system at the inlet flow rate of 0.83L/min

Fig. 7 Average temperature and temperature difference of battery modules at the inlet flow rate of 0.67L/min
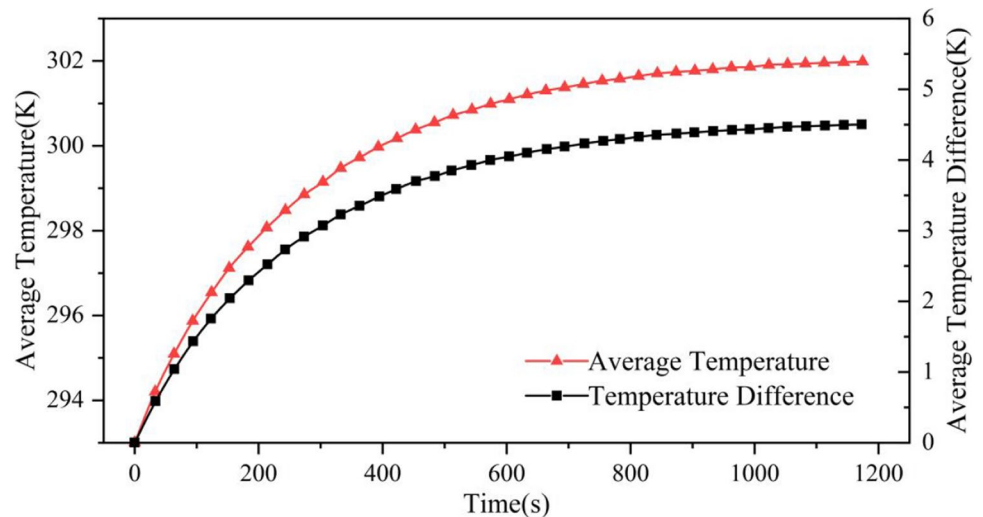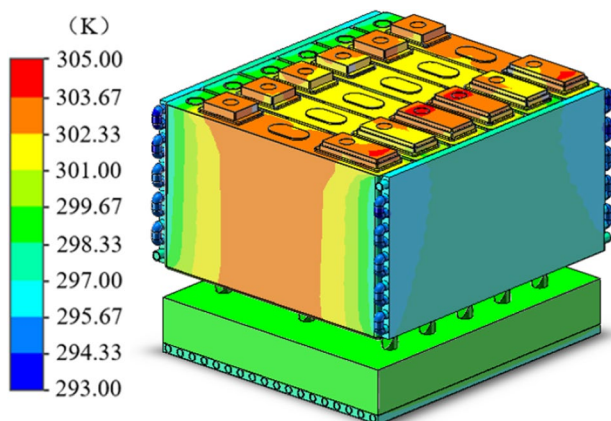

Figure 9 shows the overall average temperature and the temperature difference between the maximum and minimum temperature of the Li-ion battery module at the inlet flow rate of 0.83L/min. As shown in the figure, the overall average temperature and temperature difference trend of lithium-ion battery under the inlet flow rate of 0.83L/min is basically the same as that at the inlet flow rate of 0.67L/min and tends to be stable after 500s. When the discharge is cut off, the average temperature of the lithium-ion battery is about 301.7K, and the average temperature difference is about 4.5K.

Figure 10 is a cloud diagram of the overall temperature distribution of the thermal management system at an inlet flow rate of 0.83L/min. As shown in the figure, the overall temperature distribution of the thermal management system has little change compared to when the inlet flow

Fig. 8 Temperature distribution of TMS at the inlet liquid flow rate of 0.67L/min

rate is 0.67L/min. The temperature distribution when the liquid inlet flow rate is 0.50L/min is greatly improved compared to when the liquid flow rate is 0.33L/min. The high-temperature concentration area in the lithium-ion battery module is significantly reduced, and the overall temperature distribution is more uniform. This shows that although the increase in the liquid inlet flow rate is conducive to the improvement of heat exchange efficiency, when the liquid inlet flow rate is too high, the effect of improving the temperature distribution of the lithium-ion battery module is not obvious, as described in subsections 4.1.1 and 4.1.2. According to the calculation of velocity uniformity based on the principle of field synergy, with the increase of the inlet flow rate, the velocity uniformity coefficient γ gradually decreases, which is not conducive to the improvement of the temperature field. And as the flow rate is too high, the frictional resistance coefficient f gradually increases, which means that the thermal management system needs to consume more power.

Performance comparison of thermal management systems at different inlet liquid flows

Figure 10a shows the overall average temperature of the lithium-ion battery module as the inflow rate increases from 0.33 to 0.83L/min. As shown in the figure, the maximum temperature rise of the lithium-ion battery module decreases from 304 to 301.9K as the liquid inlet flow rate increases from 0.33 to 0.83L/min. The average temperature changes from 0.33 to 0.50L/min, while the average temperature changes from 0.50 to 0.83L/min are less than 0.3K. Figure 10b shows the temperature difference between the maximum and minimum temperature of the Li-ion battery module when the liquid intake flow rate increases from 0.33 to 0.83L/min. As shown in the figure, as the
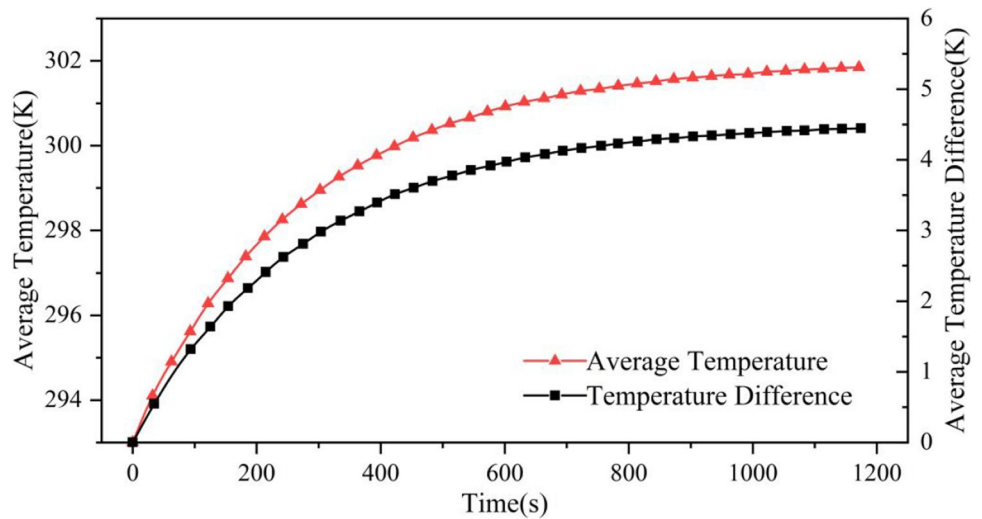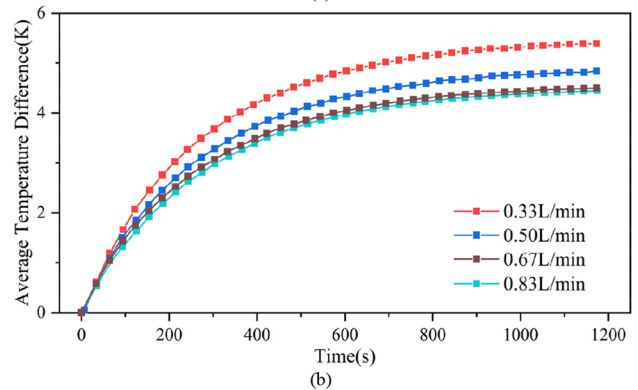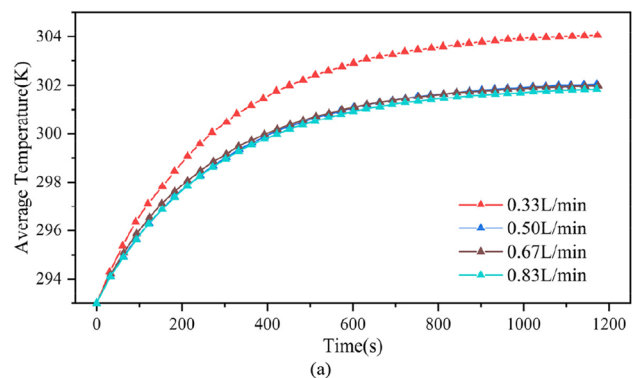
liquid inlet flow rate increases from 0.33 to 0.83L/min, the temperature difference of the lithium-ion battery module decrease from 5.4 to 4.4K. The temperature difference of the lithium-ion battery module decreases by 0.6K when the liquid flow rate increases from 0.33 to 0.50L/min; the temperature difference of the lithium-ion battery module decreases by 0.3K when the liquid flow rate increases from 0.50 to 0.67L/min; the temperature difference of the lithium-ion battery module decreases by less than 0.1K when the liquid flow rate increases from 0.67 to 0.83L/min. It can be seen that the overall thermal characteristics of the thermal management system are improved with the increase of the inlet flow rate from 0.33 to 0.83L/min.

This paper quotes the velocity uniformity fraction and the friction coefficient to analyze the overall thermal characteristics of the thermal management system of a lithium-ion battery module at different inlet flows. The velocity uniformity coefficient is used to analyze the synergy between the velocity and temperature fields. The velocity uniformity coefficient is used to analyze the synergy between the velocity field and the temperature field. The higher the velocity uniformity coefficient, the better the heat transfer performance of the fluid. As the inlet flow rate increases, the velocity uniformity coefficient of the glycol mixture in the channel liquid cooling plate becomes lower and lower. The coefficient of frictional resistance can be used to evaluate the
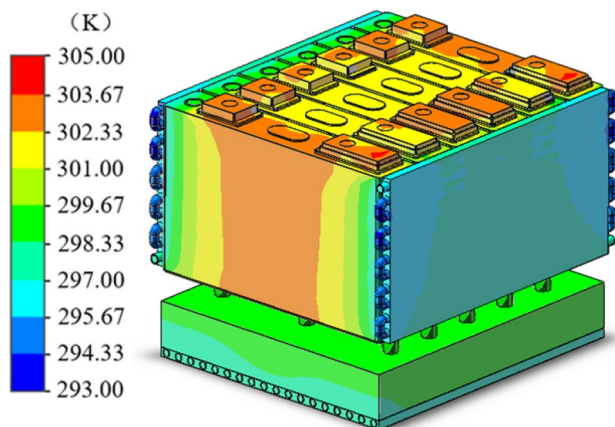
Fig. 10 Temperature distribution of TMS at the inlet liquid flow rate of 0.83L/min

Fig. 11 a Average battery pack temperature at different water inlet flows; **b** temperature difference of the battery pack at different water inlet flows

internal flow field resistance of the designed microchannel. The higher the coefficient of frictional resistance, the higher the resistance to the flow of the glycol mixture inside the microchannel liquid-cooled plate and the higher the energy consumption required; the higher the flow rate, the higher the coefficient of frictional resistance.

From Fig. 11, it can be seen that when the inlet liquid flow rate is increased from 0.67 to 0.83L/min, the temperature rises of the lithium-ion battery; the decrease in temperature difference is very small, while at this time, the frictional resistance coefficient is relatively high, and the required energy consumption is relatively high, while at this time, the frictional resistance coefficient is relatively high, and the required energy consumption is relatively high. Therefore, it is more reasonable to choose 0.67L/min as the inlet flow rate of the microchannel liquid cooling plate of the composite thermal management system.

Conclusion

This paper takes the lithium-ion battery during 3C discharge as the research object and takes the speed uniformity coefficient, friction resistance coefficient, and thermal characteristic parameters as the evaluation indicators. The thermal management system of the microchannel liquid-cooled plate at four inlet flows of 0.33L/min, 0.50L/min, 0.67L/min, and 0.83L/min was also analyzed, and the optimum inlet flow rate for the established thermal management system model was finally determined. The main conclusions are as follows.

(1) When the liquid inlet flow of the thermal management system is 0.33L/min and 0.50L/min, the average temperature rise of the lithium-ion battery module during 3C discharge is less than 308K, but the maximum temperature difference exceeds 5K, so 0.33L/min and 0.50L/min enter the liquid The flow cannot meet the heat dissipation requirements of the lithium-ion battery module during 3C discharge.

(2) When the thermal management system has a liquid inlet flow of 0.67L/min and 0.83L/min, the average temperature rise of the lithium-ion battery module during 3C discharge is less than 308K, and the maximum temperature difference is less than 5K, which can meet the heat dissipation of the lithium-ion battery module during 3C discharge demand.

(3) With the increase of the liquid inlet flow rate, the maximum temperature rise and the maximum temperature difference of the lithium-ion battery module have been reduced, and the overall thermal characteristics of the thermal management system have been improved. However, the higher the liquid inlet flow rate, the lower the corresponding speed uniformity coefficient. The

efficiency of improving the thermal characteristics of the lithium-ion battery module is also lower.

(4) Compared with the thermal management system when the inlet flow rate is 0.67L/min, the increase in the inlet flow rate of the thermal management system to 0.83L/min will affect the temperature rise of the lithium-ion battery, and the temperature difference has little effect, and the friction resistance coefficient is relatively high at this time, and the required energy consumption is relatively high. Therefore, 0.67L/min is selected as the liquid inlet flow rate of the microchannel liquid-cooled plate of the composite thermal management system.

References

1. Kwon H, Park H (2019) Numerical simulation of prismatic lithium-ion battery life cycles under a wide range of temperature[J]. Int J Precis Eng Manuf Green Technol 6(1):63–73
2. Prasad A, Parhizi M, Jain A (2019) Experimental and numerical investigation of heat transfer in Li-ion battery pack of a hoverboard[J]. Int J Energy Res
3. Donal P, Finegan Bernhard T (2017) Tracking internal temperature and structural dynamics during nail penetration of lithium-ion cells[J]. J Electrochem Soc 164(13):3285–3291
4. Tang Z, Min X, Song A et al (2019) Thermal management of a cylindrical lithium-ion battery module using a multichannel wavy tube[J]. J Energy Eng 145(1):04018072.1–04018072.9
5. Xu X, Tong G, Li R (2020) Numerical study and optimizing on cold plate splitter for lithium battery thermal management system[J]. Appl Therm Eng 167(11):114787
6. Zhou H, Zhou F, Wang Q, et al (2019) Thermal management of cylindrical lithium-ion battery based on a liquid cooling method with half-helical duct[J]. Appl Therm Eng 114257
7. Jiang Z, Qu Z (2019) Lithium-ion battery thermal management using heat pipe and phase change material during the discharge-charge cycle: a comprehensive numerical study[J]. Appl Energy 242(PT.1-1284):378–392
8. Chang C, Huang S, Chen W (2019) Thermal and solid electrolyte interphase characterization of lithium-ion battery[J]. Energy 174(May 1):999–1011
9. Cao W, Zhao C, Wang Y et al (2019) Thermal modeling of full-size-scale cylindrical battery pack cooled by channeled liquid flow[J]. Int J Heat Mass Transf 138(AUG):1178–1187
10. Martín M, Leire, Gastelurrutia J, et al (2019) Optimization of thermal management systems for vertical elevation applications powered by lithium-ion batteries[J]. Appl Therm Eng 147:155–166
11 Huo Y, Rao Z, Liu X et al (2015) Investigation of power battery thermal management by using mini-channel cold plate[J]. Energy Convers Manag 89(jan):387–395
12. Jarrett A, Kim I (2014) Influence of operating conditions on the optimum design of electric vehicle battery cooling plates[J]. J Power Sources 245(jan.1):644–655

13. Ye X, Zhao Y, Quan Z (2018) Experimental study on heat dissipation for lithium-ion battery based on micro heat pipe array (MHPA). Appl Therm Eng 130:74–82

14. Tran T, Harmand S, Sahut B (2014) Experimental investigation on heat pipe cooling for hybrid electric vehicle and electric vehicle lithium-ion battery. J Power Sources 265:262–272

15. Javani N, Dincer I, Naterer G et al (2014) Modeling of passive thermal management for electrical vehicle battery packs with PCM between cells[J]. Appl Therm Eng 73(1):307–316

16. Wilke S, Schweitzer B, Khateeb S et al (2017) Preventing thermal runaway propagation in lithium ion battery packs using a phase change composite material: an experimental study[J]. J Power Sources 340:51–59

17 Chengning Z, Xin J, Junqiu L (2017) PTC Self-heating experiments and thermal modeling of lithium-ion battery pack in electric vehicles[J]. Energies 10(4):572

18. Lei Z, Zhang Y, Lei X (2018) Improving temperature uniformity of a lithium-ion battery by intermittent heating method in cold climate[J]. Int J Heat Mass Transf 121:275–281

19. Wang Y, Wang H, Zhang Y et al (2021) Thermal oxidation characteristics for smoke particles 1 from an abused prismatic Li(Ni0.6Co0.2Mn0.2)O2 Battery 2[J]. The Journal of Energy Storage 39(1)

20. Wang Y, Gao Q, Wang H (2020) Structural design and its thermal management performance for battery modules based on refrigerant cooling method[J]. Int J Energy Res 45(9)

21. Zhang Y, Wang H , Wang Y et al (2020) Thermal abusive experimental research on the large-format lithium-ion battery using a buried dual-sensor[J]. Journal of Energy Storage 33

22. Zhang T, Gao Q, Wang G et al (2017) Investigation on the promotion of temperature uniformity for the designed battery pack with liquid flow in cooling process[J]. Appl Therm Eng 116(Complete):655–662

23. Zhu J, Sun Z, Wei X et al (2016) An alternating current heating method for lithium-ion batteries from subzero temperatures[J]. Int J Energy Res 40(13):1869–1883

24. Qu Z, Jiang Z, Wang Q (2019) Experimental study on pulse self-heating of lithium-ion battery at low temperature[J]. Int J Heat Mass Transf 135(JUN):696–705

25. Panchal S, Dincer I, Agelin M, Fowler M et al (2016) Experimental and theoretical investigation of temperature distributions in a prismatic lithium-ion battery[J]. Int J Therm Sci 99:204-212

26. Melcher A, Ziebert C, Rohde M et al (2016) Modeling and simulation the thermal runaway behavior of cylindrical Li-ion cells—computing of critical parameter [J]. Energies 9(4):292

27. Fu J, Xu X, Li R (2019) Battery module thermal management based on liquid cold plate with heat transfer enhanced fin[J]. Int J Energy Res 43(8):4312–4321

28. Babapoor A, Azizi M, Karimi G (2015) Thermal management of a Li-ion battery using carbon fiber-PCM composites[J]. Appl Therm Eng 82:281–290

29. Bernardi D, Pawlikowski E, Newman J (1985) A general energy balance for battery systems[J]. J Electrochem Soc 132(1):5–12